Facile synthesis of NFL-ZnWO$_4$ for pseudocapacitor applications

Xiao Fan, and *Xuyuan* Chen[*]

Department of Microsystems, University of South-Eastern Norway, Campus Vestfold, Raveien 215, 3184Borre, Norway

Abstract. In this report, NFL-ZnWO$_4$ was synthesized by a hydrothermal route and investigated for application in supercapacitors for the first time. The physical and chemical characterizations of the prepared nanomaterial were analyzed by SEM, EDS, XRD and XPS, respectively. Supercapacitors study of CV, GCD and EIS revealed that NFL-ZnWO$_4$ exhibits good electrochemical properties. The high specific capacitance value of 107.7 F g^{-1} was achieved at 5 mV s^{-1}. These findings demonstrated that ZnWO$_4$ could be a promising electrode material candidate and highly desirable for application of high property supercapacitors in the future.

1 Introduction

With the development of human society, a large amount of energy sources have been consumed, such as coal, petroleum, and natural gas [1]. Therefore, novel and suitable energy storage devices need to be developed. Supercapacitors(SCs), the new devices between conventional physical capacitors and lithium-ion batteries, have been extensively studied to serve as one of the most promising candidates for energy storage because of their high power density, long cycling lifespan and fast charge/discharge process [2]. In general, supercapacitors can be divided into two categories according to the energy storage mechanism: one is the electric double layer capacitors(EDLCs), in which carbonaceous materials have been widely utilized and the other is the Faradaic redox reaction pseudocapacitors(PsCs) usually containing transition metal oxides as the electrode materials [3]. In comparison with electric double layer capacitors, pseudocapacitors show much higher specific capacitance performance, making it is of far-reaching significance to focus research on [4].

So far, nanostructured metal oxides have been intensively explored in order to use them as electrode materials. However, the high cost of some transition metal oxides limited their practical use in commercial supercapacitors. Hence, searching for a low cost pseudocapacitive material and economically affordable generation systems has been a major challenge in supercapacitors research [5, 6]. In recent years, Zinc tungstate(ZnWO$_4$), an environmentally friendly low cost transition metal oxide and both its constituent elements being relatively earth-abundant [7], with high technological applications in

---

[*] Corresponding author: Xuyuan.Chen@usn.no

various fields, such as photocatalysts, optical fibers and gas sensors [8, 9], have been reported. Because both Zn and W elements can take part in the Faradaic redox reactions, $ZnWO_4$ is of great potential for electrode materials [10]. Unfortunately, $ZnWO_4$ is rarely reported as the composite materials for supercapacitors [11].

Herein, we employed a simple, facile and effective hydrothermal route to synthesize nanoflower-like $ZnWO_4$(NFL-$ZnWO_4$) and to the best of our knowledge, there are no reports on this morphology. Moreover, its application in supercapacitors was systematically studied. The present results demonstrated the NFL-$ZnWO_4$ can be considered as a promising candidate for pseudocapacitor applications. In addition, to fulfill the increasing demands, a rational modification of $ZnWO_4$ nanostructure and compositing $ZnWO_4$ with other electrode materials are both advisable.

2 Experimental

2.1 Chemicals

Zinc nitrate hexahydrate($Zn(NO_3)_2 \cdot 6H_2O$), sodium tungstate dehydrate($Na_2WO_4 \cdot 2H_2O$), ammonium fluoride(NH_4F), hydrogen chloride solution, absolute ethanol, acetylene black, polyvinylidene fluoride (PVDF) and potassium hydroxide(KOH) were purchased from Sigma-Aldrich. All the chemicals were of analytical grade and were used as received without further purification.

2.2 Sample preparation

The $ZnWO_4$ was obtained by a simple and facile hydrothermal method. Briefly, 1 mmol of $Zn(NO_3)_2 \cdot 6H_2O$, 1 mmol of $Na_2WO_4 \cdot 2H_2O$, and 8 mmol of NH_4F were dissolved in 50 mL deionized(DI) water and stirred vigorously for 60 min to form a milky suspension. Then, the suspension was transferred into a Teflon-lined stainless steel autoclave. Subsequently, the sealed autoclave was heated at 120 ℃ for 8 h. After cooling to room temperature naturally, the collected precipitate was washed with DI water and dried at 90 ℃ for 12 h. Finally, the as-prepared product was heat treated at 600 ℃ for 6 h in a muffle furnace.

2.3 Electrodes fabrication

Before the fabrication, the nickel foam(NF) was carefully cleaned with 3 M HCl, absolute ethanol and DI water for 30 min in an ultrasonic bath, respectively, and dried in a vacuum oven at 50 ℃. The working electrode was prepared by mixing an electro-active material, acetylene black and PVDF with a ratio of 75:15:10. The mixture were continuously grinded for 10 min in a mortar and pressed on NF finally.

2.4 Materials characterization

X-ray powder diffraction(XRD) characterization was performed using a DRIGC-Y 2000A with Cu-Kα_1 radiation ($\lambda = 1.5406$ Å) and the scanning speed was 6° min^{-1}. A Hitachi SU-3500 scanning electron microscope(SEM) equipped with an energy-dispersive X-ray spectrometer(EDS) was used to observe the morphologies and analyse the element compositions of material. X-ray photoelectron spectroscopy(XPS) measurement was carried out on an ESCALAB 250Xi.

2.5 Electrochemical measurement

Three-electrode system was employed to study the supercapacitor behavior of fabricated working electrode using a Zahner IM6 electrochemical workstation, in which Pt wire and Ag/AgCl (in saturated KCl) were used as a counter electrode and a reference electrode, respectively. Cyclic voltammogram(CV), galvanostatic charge/discharge(GCD) and electrochemical impedance spectra (EIS) measurements were conducted in 2M KOH electrolyte.

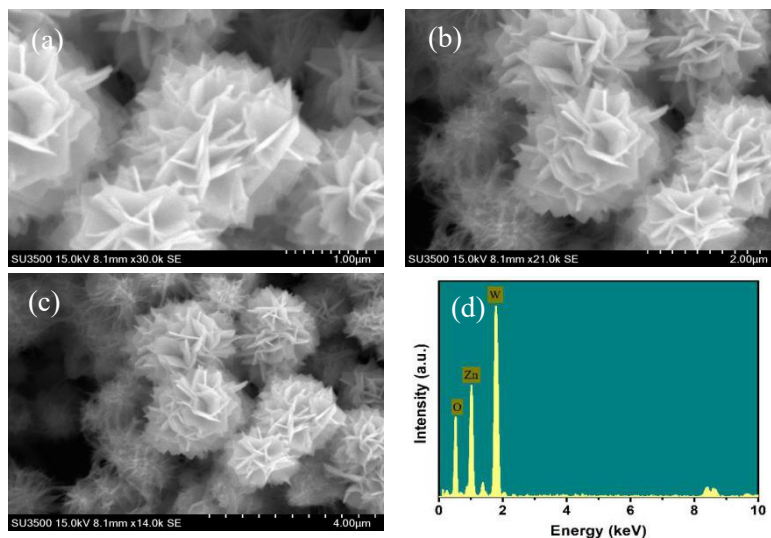The gravimetric specific capacitance (C_s) based on CV is defined as

$$C_s(CV) = \frac{1}{2mv\Delta V} \int i(V)dV \qquad (1)$$

The gravimetric specific capacitance based on GCD is given by

$$C_s(GCD) = \frac{It}{m\Delta V} \qquad (2)$$

$\int i(V)dV$ is the integrated area of CV curve, and m, ΔV, v, I, t are the mass of active materials, potential window, scan rate, discharge current and discharge time.

3 Results and discussion

**Fig. 1.** SEM images(a-c) and EDS spectrum(d) of the synthesized $ZnWO_4$.

Figure 1a-c presents the typical SEM images with different magnification to illustrate the morphologies of the synthesized $ZnWO_4$. It clearly reveals that the $ZnWO_4$ exhibits a well-defined flower-like structure and was composed of layered and uniform nanoflakes. Meanwhile, the nanoflakes with diameters ranging from 1 to 2 μm intersect among each other. The macropores of the nanoflower structure, which are formed by stacking of the nanoflakes, are very suitable for ionic transport in the electrode of a supercapacitor [12]. In addition, the elemental composition was characterized by EDS, as shown in Figure 1d. The peaks correspond to O, Zn, and W elements. No other impurity element was observed, indicating the high purity of the samples.

The crystal structure of the obtained $ZnWO_4$ was analyzed by XRD, as shown in Figure 2. The obvious and typical reflection diffraction peaks correspond to (010), (100), (011), (110), (111), (021), (200), (121), (130), (-221) and (113) planes respectively. All the peaks can be indexed and well-matched to the monoclinic wolframite $ZnWO_4$ with the standard card (JCPDS card no.15-0774, space group $P2/c$), which also indicates that no other

impurities exist. Moreover, the strong and sharp peaks at (1 1 1), (1 0 0), and (0 2 1) planes suggest that the as-prepared $ZnWO_4$ samples are highly crystalline [13].
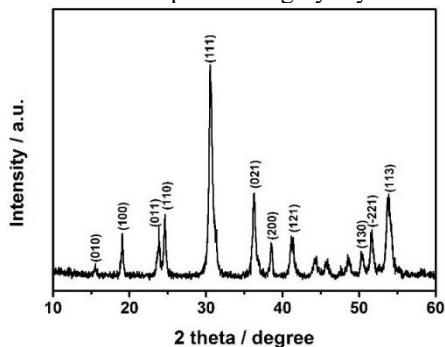

Fig. 2. XRD patterns of the as-prepared $ZnWO_4$ sample.
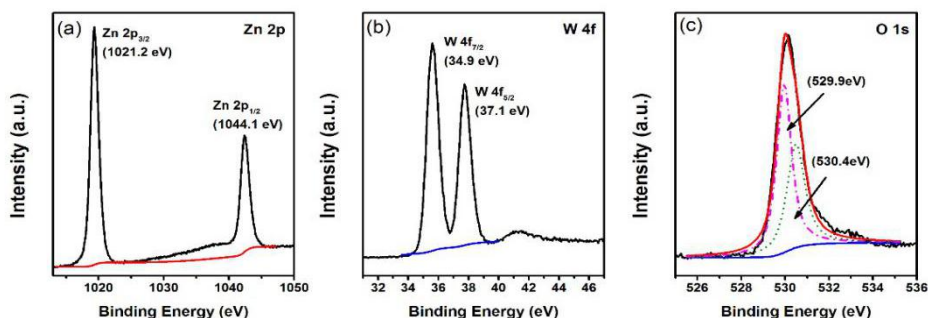
Fig. 3. High-resolution XPS survey spectra of $ZnWO_4$: (a) Zn 2p region, (b) W 4f region, and (c) O 1s region.

To further determine the elemental composition and chemical valance state, XPS was conducted on the $ZnWO_4$. The Zn 2p, W 4f, O 1s core-level XPS spectra of the $ZnWO_4$ are plotted in Figure 3. The Zn $2p_{3/2}$ and Zn $2p_{1/2}$ peaks at binding energies of ˜ 1021.2eV and ˜ 1044.1eV on a high resolution scan are shown in Figure 3a. This splitting is due to spin orbit coupling of Zn 2p states [8]. Similarly, Figure 3b illustrates the high-resolution spectrum of W 4f. The doublets of W $4f_{7/2}$ and W $4f_{5/2}$ peaks appears at binding energies of ˜ 34.9eV and ˜ 37.1eV respectively. Figure 3c displays the O 1s spectrum. The O 1s region can be fitted by two peaks located at ˜ 529.9eV and ˜ 530.4eV, which can be ascribed to the O^{2-} in the $ZnWO_4$ and hydroxyl groups on the surface of the sample [14]. All peaks at specific binding energies are well consistent with previous works [15] and clearly confirm the successful synthesis of $ZnWO_4$ nanomaterial.

The electrochemical performances of the fabricated electrode were deeply investigated. Figure 4a reveals the CV curves within the potential window of 0–0.5 V at various scan rates ranging from 5 to 100 mV s^{-1}. As expected, the CV at different scan rates exhibits a similar shape and a pair of strong redox peaks, which indicates the ideal capacitive behaviors and the capacitance characteristics are mainly governed by Faradaic redox reactions. This reaction is based on the reversible redox of Zn^{2+}–Zn^{3+}. The specific capacitance of 107.7 F g^{-1} can be calculated by equation(1) at scan rate of 5 mV s^{-1} further. Obviously, the anodic and the cathodic peaks shift to higher and to lower potentials with the increase of scan rate, respectively. It can be explained by the kinetic limitation of the redox reaction [16], which leads to a lower specific capacitance, as shown in Figure 4b.
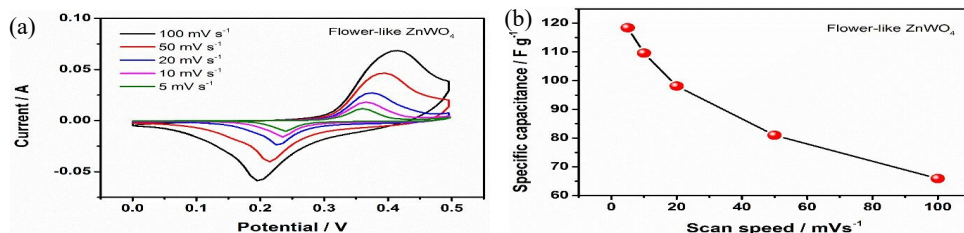
Fig. 4. (a) CV curves and (b) specific capacitance based on CV.

Figure 5a demonstrates the GCD measurements conducted at various current densities to get more information about the capacitive property. In comparison with a straight and flat line, the discharge curves displayed a significant deviation and plateau. It suggests the typical pseudocapacitive characteristics. Due to the incremental potential drop and the relatively insufficient active material involved in redox reaction under higher current densities [7], the specific capacitances achieved by equation(2) gradually decreases with the increase of current density, as can be observed from Figure 5b. The ions(OH^-) at a low current density have adequate time to transfer at the interface between the electrode and electrolyte than at a high current density [5].
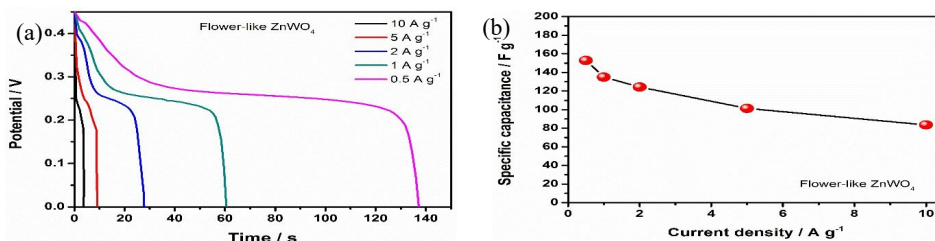
Fig. 5. (a) GCD curves and (b) specific capacitance based on GCD

EIS study was performed in Figure 6 to determine the conductive nature. At the high frequency regions, the Nyquist plot exhibits a negligible semicircle, suggesting a low charge transfer resistance and interfacial resistance between current collector and electroactive material [8]. In the low frequency regions, the plot presents a straight line with a quasi slope of 45°, indicating the more electrolyte ion diffusion to the electroactive materials [8]. In general, all features of the Nyquist plot declare the good conductivity and capacitive behavior.
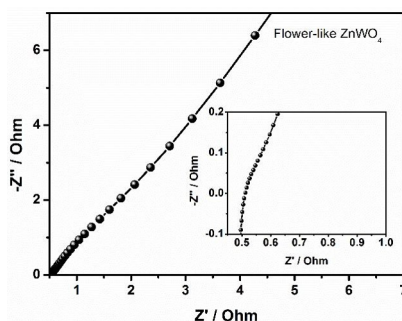
Fig. 6. EIS study.

4 Conclusion

In summary, a NFL-$ZnWO_4$ material with a unique and open-up network structure formed by interconnected nanoflakes was prepared via a hydrothermal method following an

appropriate heat treatment for the first time. The physical and chemical properties were carried out by SEM, EDS, XRD and XPS, respectively. A series of electrochemical tests including CV, GCD and EIS were conducted. It was demonstrated that the NFL-ZnWO$_4$ exhibits good electrochemical behaviors with a high specific capacitance of 107.7 F g^{-1} at 5 mV s^{-1}. In the future, efforts of morphology tunnings or synergies with other materials on ZnWO$_4$ can be made to match the superior electrochemical properties need. In view of this, ZnWO$_4$ as an electrode material is well worth being applied to supercapacitors.

Acknowledgements

References

1. Pu J, Tong Y, Wang S, Sheng E and Wang Z 2014 *Journal of Power Sources*. **250** 250-256

2. Wang C, Zhou E, He W, Deng X, Huang J, Ding M, Wei X, Liu X and Xu X 2017 *Nanomaterials*. **7(2)** 41

3. Wang Q, Wang X, Liu B, Yu G, Hou X, Chen D and Shen G 2013 *Journal of Materials Chemistry A.* **1(7)** 2468-2473

4. Qiu M, Sun P, Shen L, Wang K, Song S, Yu X, Tan S, Zhao C and Mai W 2016 *Journal of Materials Chemistry A.* **4(19)** 7266-7273

5. Kumar R D, Andou Y and Karuppuchamy S 2016 *Journal of Physics and Chemistry of Solids*. **92** 94-99

6. Yang Y, Zhu J, Shi W, Zhou J , Gong D, Gu S, Wang L, Xu Z and Lu B 2016 *Materials Letters*.**177** 34-38

7. Guan B, Hu L, Zhang G, Guo D, Fu T, Li J, Duan H, Li C and Li Q 2014 *RSC Advances.* **4(9)** 4212-4217

8. Ede S R, Ramadoss A, Nithiyanantham U, Anantharaj S and Kundu S 2015 *Inorganic chemistry*. **54(8)** 3851-3863

9. Shim H W, Cho I S, Hong K S, Lim A H and Kim D W 2011 *Journal of Physical Chemistry C.* **115(32)** 16228-16233

10. Luo L, Liu T, Zhang S, Ke B, Yu L, Hussain S and Lin L 2017 *Ceramics International.* **43(6)** 5095-5101.

11. Han S, Lin L, Zhang K, Luo L, Peng X and Hu N 2017 *Materials Letters*. **193** 89-92

12. Tang Y, Liu Y, Yu S, Zhao Y, Mu S and Gao F 2014 *Electrochimica Acta*. **123** 158-166

13. Huang Y, Gao Y, Zhang Q, Cao J J, Huang R J, Ho W and Lee S C 2016 *Applied Catalysis A: General*. **515** 170-178

14. Yu C and Jimmy C Y 2009 *Materials Science and Engineering: B*. **164(1)** 16-22

15. Khyzhun O Y, Bekenev V L, Atuchin V V, Galashov E N and Shlegel V N 2013 *Materials Chemistry and Physics*. **140(2-3)** 588-595

16. Lu P, Müller L, Hoffmann M and Chen X 2017 *Nano Energy*. **41** 618-625